Biochimica et Biophysica Acta 1817 (2012) 579–589

Contents lists available at SciVerse ScienceDirect

Biochimica et Biophysica Acta

journal homepage: www.elsevier.com/locate/bbabio

Review

Structural studies on bovine heart cytochrome *c* oxidase ☆

Shinya Yoshikawa *, Kazumasa Muramoto, Kyoko Shinzawa-Itoh, Masao Mochizuki

Department of Life Science, University of Hyogo, Hyogo 678-1297, Japan

ARTICLE INFO

Article history:
Received 29 September 2011
Received in revised form 16 December 2011
Accepted 29 December 2011
Available online 4 January 2012

Keywords:
X-ray structural analyses
Membrane proteins
Hemoproteins
Bovine cytochrome *c* oxidase
O_2 reduction
Proton pump

ABSTRACT

Among the X-ray structures of bovine heart cytochrome *c* oxidase (CcO), reported thus far, the highest resolution is 1.8 Å. CcO includes 13 different protein subunits, 7 species of phospholipids, 7 species of triglycerides, 4 redox-active metal sites (Cu_A, heme *a* (Fe_a), Cu_B, heme a_3 (Fe_{a3})) and 3 redox-inactive metal sites (Mg^{2+}, Zn^{2+} and Na^+).

The effects of various O_2 analogs on the X-ray structure suggest that O_2 molecules are transiently trapped at the Cu_B site before binding to Fe^{2+}_{a3} to provide O_2^-. This provides three possible electron transfer pathways from Cu_B, Fe_{a3} and Tyr244 via a water molecule. These pathways facilitate non-sequential 3 electron reduction of the bound O_2^- to break the O–O bond without releasing active oxygen species.

Bovine heart CcO has a proton conducting pathway that includes a hydrogen-bond network and a water-channel which, in tandem, connect the positive side phase with the negative side phase. The hydrogen-bond network forms two additional hydrogen-bonds with the formyl and propionate groups of heme *a*. Thus, upon oxidation of heme *a*, the positive charge created on Fe_a is readily delocalized to the heme peripheral groups to drive proton-transport through the hydrogen-bond network. A peptide bond in the hydrogen-bond network and a redox-coupled conformational change in the water channel are expected to effectively block reverse proton transfer through the H-pathway. These functions of the pathway have been confirmed by site-directed mutagenesis of bovine CcO expressed in HeLa cells. This article is part of a Special Issue entitled: Respiratory Oxidases.

1. Introduction

Bovine heart cytochrome *c* oxidase (CcO) was first solubilized and isolated from the mitochondrial inner membrane 70 years ago [1]. Prior to development of site-directed mutagenesis, bovine heart CcO was the most extensively studied CcO. Presently, fewer research groups use bovine heart CcO in their research projects because bacterial CcOs are amenable to site-directed mutagenesis. On the other hand, bovine heart CcO is well suited for structural and functional studies because bovine heart mitochondria provide highly pure and stable preparations of CcO in high yield. Thus, the X-ray structure of bovine heart CcO has the highest resolution among the various X-ray structures of terminal oxidases [2]. It should be noted that functional studies of any protein are generally rate-limited by the resolution of its X-ray structure. Furthermore, the site-directed mutagenesis approach is now applicable for functional studies of bovine CcO because a gene expression system has been developed [3,4].

In this article, recent progress in structural studies of bovine heart CcO is reviewed to discuss our present understanding of its reaction mechanism.

2. Basic structures of bovine heart CcO

2.1. Protein moiety

Long before the X-ray structure of bovine heart CcO was determined, the presence of 13 different subunits was proposed on the basis of SDS-PAGE analyses [5]. However, SDS-PAGE analysis was unable to determine which bands are due to intrinsic subunits or to co-purified subunits. Thus, the presence of 13 different subunits in the X-ray structure of bovine heart enzyme [6], consistent with the SDS-PAGE results, strongly supports the original proposal that bovine CcO is composed of 13 different subunits [5]. However, it should be noted that for complete verification of the proposal, the physiological roles of all subunits must be identified, since it is possible that co-purified proteins are specifically bound to CcO and co-crystallized.

The 3 largest subunits encoded by mitochondrial genes are surrounded by 10 nuclear-coded subunits [6]. The subunit arrangement is shown in Fig. 1. Subunit I, the largest subunit, contains 3 redox-active metal sites including a six-coordinated low spin heme (heme *a*), a five-coordinated high spin heme in the reduced state (heme a_3) and a mononuclear copper site in a trigonal planar coordination

☆ This article is part of a Special Issue entitled: Respiratory Oxidases.

* Corresponding author. Tel.: +81 791 58 0190; fax: +81 791 58 0489.
E-mail addresses: yoshi@sci.u-hyogo.ac.jp (S. Yoshikawa), muramoto@sci.u-hyogo.ac.jp (K. Muramoto), shinzawa@sci.u-hyogo.ac.jp (K. Shinzawa-Itoh), mochizuk@sci.u-hyogo.ac.jp (M. Mochizuki).

0005-2728/$ – see front matter © 2011 Published by Elsevier B.V.
doi:10.1016/j.bbabio.2011.12.012

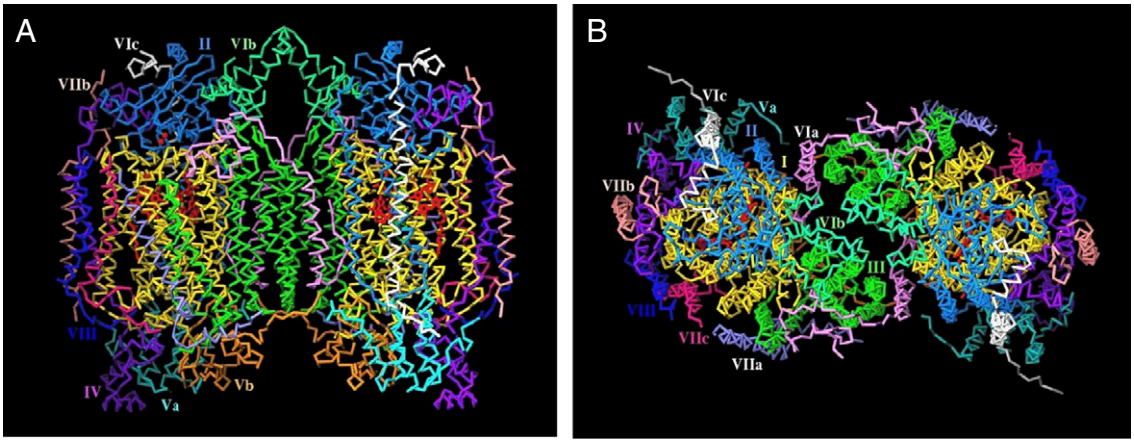

Fig. 1. The Cα backbone trace of the dimer of bovine heart CcO at 2.8 Å resolution.(A) A view of the transmembrane surface and (B) a view from the cytosolic side.

with three histidine imidazole groups (Cu_B). The third largest subunit (subunit II) contains a dinuclear copper site with cupredoxin-type coordination with two cysteine residues bridging the two atoms. Each of these four metal sites receives one-electron equivalent reversibly. Heme a_3 (or Fe_{a3}) is the site for O_2 binding when it is in the reduced state and acts as the O_2 reduction site in conjunction with Cu_B which is located nearby. The electron equivalents for the O_2 reduction are transferred from cytochrome *c* (on the positive side phase of mitochondrial membrane) via the two other metal sites, Cu_A and heme *a*. Thus, the roles of subunits I and II are obvious. Subunit III, the second largest subunit, has no metal sites, but contains a possible O_2 pathway. It was found that binding of dicyclohexylurea to Glu90 in the pathway completely inhibits O_2 reduction activity [7]. Presently, the roles of the other 10 subunits are essentially unknown. However, the fact that the resolution of the X-ray structure of bovine heart CcO is significantly higher than those of bacterial enzymes reported thus far [2] suggests that these 10 nuclear-coded subunits play roles in stabilizing the conformation and assembly of the 3 core subunits to provide stable crystals. Bacterial CcOs do not contain these subunits.

2.2. Lipids

It has been known for many years that bovine heart CcO contains a significant amount of phospholipids as intrinsic components [8]. However, for complete structural determination of these lipids, non-specifically bound (or contaminant) lipids must be completely removed. Furthermore, fairly large amounts of completely purified CcO are required for accurate structural analyses. Fortunately, the method of crystallizing bovine heart CcO, which is the best method for removal of contaminant lipids, has been well established to provide sufficient amount of crystalline CcO for lipid structural analyses. However, conditions for quantitative extraction of lipids from the protein and for quantitative determination of each lipid have not been established. Thus, a high resolution X-ray structure must be used for quantification of each lipid by fitting the lipid structure to the electron density. The complete determination of the intrinsic lipids of bovine heart CcO was published in 2007 [7].

The structures of each fatty acid tail (the chain length and the positions of the unsaturated bonds) were determined by mass spectrometry (MS) and tandem mass spectrometry (MS–MS). The positions of the fatty acyl group in the glycerol backbone of the lipids were determined by phospholipase A_2 treatment. Using these methods, 7 species of phospholipids including cardiolipin (CL), phosphatidylethanolamine (PE), phosphatidylcholine (PC), choline plasmalogen (CP), phosphatidylglycerol (PG) and 7 species of triglyceride (TG) were identified for lipid fractions extracted from crystalline bovine heart CcO and are shown in Fig. 2. The configurations of the unsaturated bonds in vaccenate and oleate were determined by GC analysis of their methyl esters prepared by solvolysis. The *cis*/*trans* ratio for vaccenate is approximately 13:1 while no *trans* configuration is detectable for oleate. The major configuration is expected to be *cis* in other unsaturated fatty acid tails. It should be noted that 4 species of choline-containing phospholipids are included and that vaccenate (Δ^{11}-octadecenoate) is included in PG in spite of the large abundance of oleate (Δ^{9}-octadecenoate), a closely-related fatty acid.

The lipid structures fit well within the electron density map of the 1.8 Å resolution X-ray structure which indicates 2CLs, 1PC, 3PEs, 4PG and 3TGs as shown in Fig. 3 [7]. The X-ray structure indicates that four phospholipids (CL1, PE1, PE3 and PG3 in Fig. 3) bridge both monomers to stabilize the dimmer state. Especially, the hydrophobic interactions between the four fatty acyl groups of CL1 and the protein surfaces of both monomers suggest that CL1 critically controls the dimmer/monomer equilibrium in the mitochondrial inner membrane.

Although, as described above, 4 species of choline-containing phospholipids are analytically identified in the crystalline CcO sample, only one site for the choline-containing phospholipids is identified in the X-ray structure. At this resolution it is impossible to identify the phospholipid species bound to the choline-containing phospholipid site. The binding specificity of the site could be determined only by determining the head group structure. Regardless of the structure of the fatty acid tails, these four choline-containing phospholipids species have equal affinity for the site. The other interpretation is that site specificity is determined by the structure of the fatty acyl tail portion. Thus, only one of the 4 choline-containing phospholipids is selectively bound to the site. Consistent with this interpretation, each of the other three phospholipids has a single set of fatty acyl groups although there is more than one binding site. Namely, if the head group identifies the binding site and if each phospholipids has several sets of fatty acid tails in its pool (mitochondrial inner membrane), the crystalline sample must contain more than one species of phospholipids.

In order to determine which part of the phospholipid (the head group or the fatty acyl tail) recognizes its binding site, the phospholipid content of the mitochondrial membrane was determined by the same method used for the enzyme preparation. The analyses show that the composition of the phospholipids is identical to that of crystalline bovine CcO. That is, the pool for these phospholipids is composed of only a single species for each of the 3 phospholipids, CL, PE and PG, which has more than one binding sites as described above. These results strongly suggest that the head groups of the phospholipids recognize their binding sites. Three binding sites for TG were identified in the X-ray structure, while 7 species of TG were identified by MS and GC analyses for solvolyzed fatty acid

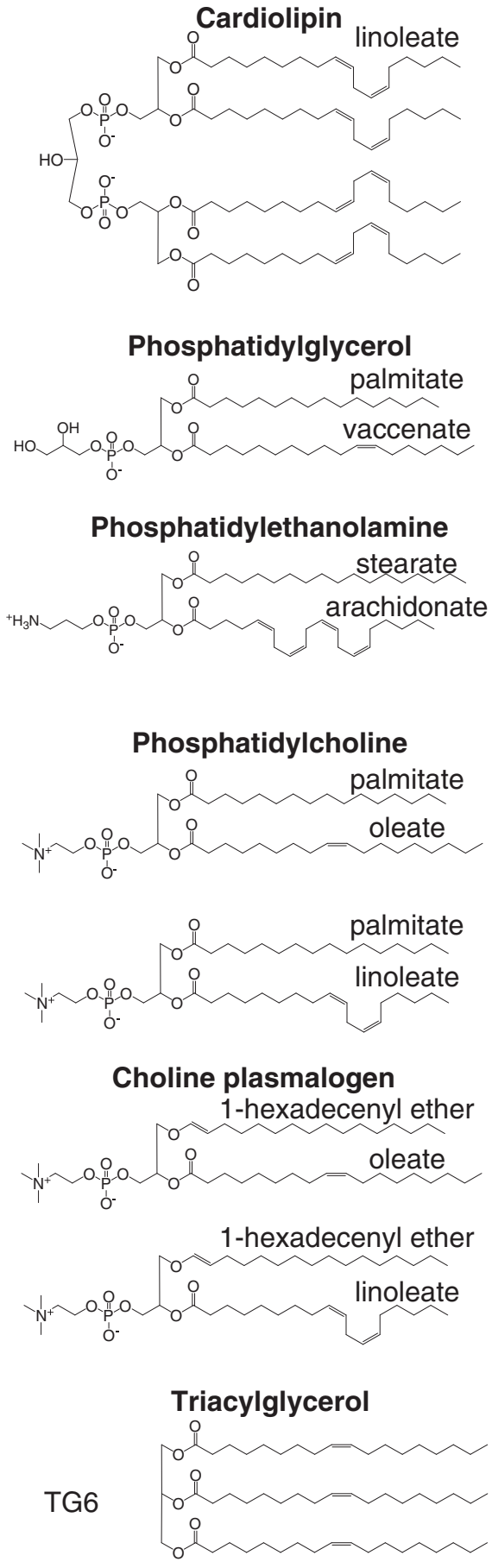

methyl esters. Again, the lipid pool contains only the 7 TG species, suggesting that the head group or the fatty acyl group at the terminal carbon of the glycerol backbone recognizes the TG binding site [7].

The configuration of vaccenate was characterized for the lipid extract from the mitochondrial inner membrane. A *cis*/*trans* ratio of 5:1 was determined. This result, together with the *cis*/*trans* ratio of 13:1 for CcO, indicates that the *cis*-configuration is selected by CcO as being more favorable than the *trans*-configuration. The electron densities for the two vaccenate molecules in subunit III are clear enough to conclude that the unsaturated bond is 100% in the *cis*-configuration [7]. Thus, subunit III identifies the *cis*-vaccinate against the *trans*-vaccenate, which strongly suggests a critical role in this enzyme function.

The total amount of fatty acyl groups, determined by quantitative analysis of the solvolysate of the lipid extract using tripentadecanoic glyceride (an unnatural TG), as an internal standard showed 30.6 (±3.4) fatty acyl groups other than arachidonate per molecule of CcO (n = 6) [7]. Phosphorous analysis of 40 different batches of the crystalline preparation provided 12.9 (±1.9) phosphorous atoms per CcO molecule. The number of fatty acid tails and phosphorous atoms determined experimentally are consistent with the total number of the tails detectable in the X-ray structure. This shows that all of the lipids specifically bound to CcO which are detectable in the X-ray structure are extracted quantitatively. Thus, the crystalline CcO preparation does not contain non-specifically bound lipids [7].

X-ray structural analysis of the dicyclohexylurea (DCU)-bound form of CcO reveals that the DCU unit bound to Glu90, within the possible O_2 pathway of subunit III, induces significant conformational changes in the two palmitate tails of PGs without producing a significant structural change in the protein moiety to effectively block the pathway [7]. The conformational changes in palmitate tails are independent of the protein conformation. This suggests that the palmitate tails are able to actively control the O_2 transfer in response to the flow of O_2 through the pathway. Interestingly, a bacterial CcO preparation depleted of subunit III shows suicide inhibition characterized by decreased enzymatic activity which is induced by repeated enzymatic turnover [9]. This suggests that subunit III controls the rate of supply of O_2 to the O_2 reduction site to prevent the formation of reactive oxygen species [7].

2.3. Complete determination of the structure of heme A

Heme A (the heme moiety of hemes *a* and a_3) is significantly larger and less stable than protoheme. Thus, its structure was not determined until 1975 [10]. However determination of the absolute configuration of the single chiral center of heme A (the carbon with the OH substituent within the hydroxyfarnesylethyl group) using standard methods was not attempted because crystallization of heme A and synthesis of heme A for determination of the absolute configuration are quite challenging. The absolute configuration was finally identified in 2005 to be the *S*-configuration in a newly developed X-ray structural analysis for heme A in CcO crystals [11].

3. Structural studies on the O_2 reduction and proton pumping system of bovine heart CcO

3.1. Structural analyses of the O_2 reduction system

One-electron reduction of molecular oxygen (O_2) is energetically unfavorable, while two electron reduction is quite favorable. Thus, the two transition metals in the O_2 reduction site appear to be

Fig. 2. Chemical structures of lipids detected in crystalline bovine heart CcO.The major configurations (*cis*) for vaccenate and oleate are shown. For the other unsaturated fatty acids, the *cis*-configuration is assigned provisionally. One of the possible structures of TG bound to bovine heart CcO is shown.

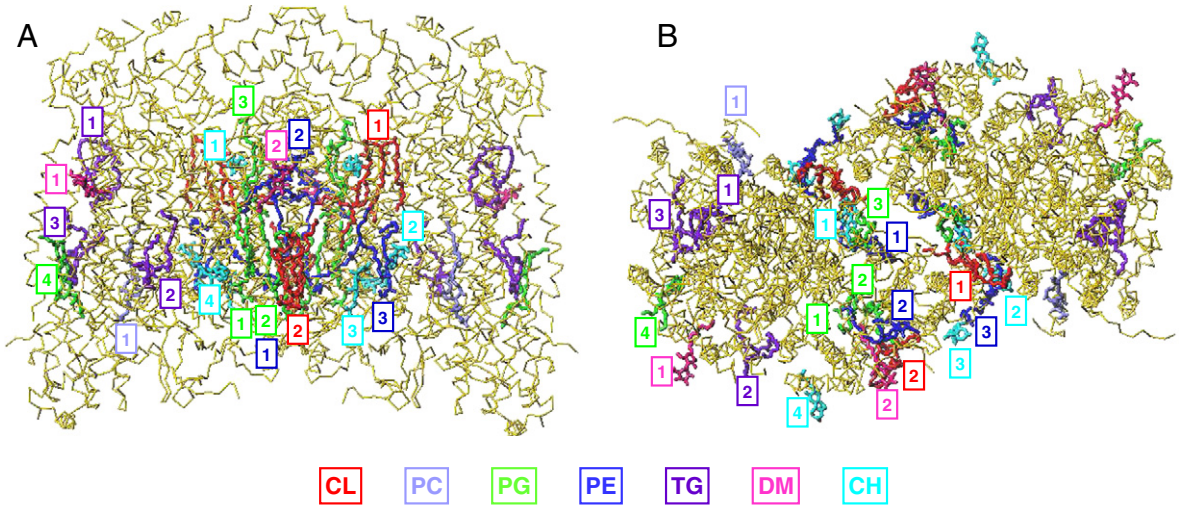

Fig. 3. The locations of lipids and detergents in the X-ray structure of bovine heart CcO at 1.8 Å resolution in the oxidized state. (A) Top and (B) side views.CH and DM denote cholate and decylmaltoside, respectively. Association of lipids and detergents with individual monomers is indicated by arbitrarily-numbered rectangles.

suitable for the two-electron reduction of O_2. However, it was unexpectedly found in resonance Raman analyses that the initial intermediate is an O_2-bound form known as intermediate A [Fe_{a3}^{2+}-O_2, Cu_B^{1+}] [12]. Furthermore, the resonance Raman band of the second intermediate shows that the O – O bond is cleaved in the transition to provide intermediate P [$Fe_{a3}^{5+}=O^{2-}$, Cu_B^{2+}-OH^-] in which Fe_{a3}^{5+} denotes the formal oxidation state of Fe_{a3} [12]. Decomposition of peroxide, one-electron reduction of which is energetically favorable, is expected to be much faster than its formation, although the peroxide structure for the second intermediate was postulated for many years before the resonance Raman finding. The one-oxidation equivalent is likely to be located on the OH group of Tyr244 which is very close to the heme-copper system. Electrons are then sequentially transferred from cytochrome *c* via Cu_A and heme *a*, to provide intermediates F [$Fe_{a3}^{4+}=O^{2-}$, Cu_B^{2+}-OH^-], O [Fe_{a3}^{3+}-OH^-, Cu_B^{2+}-OH^-], E [Fe_{a3}^{3+}-OH^-, Cu_B^{1+}] and R [Fe_{a3}^{2+}, Cu_B^{1+}] [2]. The one-step transition from A to P suggests that this strategy enables cleavage of the O – O bond (involving complete reduction), without releasing any reactive oxygen species. The reaction cycle was established almost 20 years ago [12]. However, no structural basis for the reaction cycle has been identified. Resonance Raman analysis is a very powerful tool for identification of the structure of a heme bound-ligand. However, it provides essentially no structural information with respect to the O_2 reduction site. Thus, X-ray structural analyses of these intermediate species are desirable for elucidation of the O_2 reduction mechanism. However, most of these intermediate species are unstable and unsuitable for crystallization. Thus, the functions of the O_2 reduction site have been probed by high resolution X-ray structural analysis of CcO derivatives with various stable O_2 analogs.

The X-ray structure of NO-bound, fully reduced CcO at 1.8 Å resolution shown in Fig. 4A indicates that the best O_2 analog, NO, binds to Fe_{a3}^{2+} in a bent end-on fashion. However, the distance between Cu_B^{1+} and the bound ligand is 2.5 Å, suggesting a very weak interaction. Furthermore, Cu_B^{1+} has trigonal planar coordination with three histidine imidazole groups. The structure strongly suggests that Cu_B^{1+} is very stable and thus is a poor electron donor as well as a poor ligand acceptor. The coordination structure and the distance between Cu_B and the external ligand distance strongly suggest that Cu_B is unlikely to act as the second electron donor [13]. Tyr244 is covalently linked to His240, one of the imidazole groups coordinated to Cu_B [14]. This tyrosine residue is located near the external ligand bound to Fe_{a3}^{2+}. A deprotonated Tyrosine-OH group will often function as a transition metal by providing reversible donation of electrons. Thus, this Tyr244 could function as the second electron donor to the O_2 bound to Fe_{a3}^{2+}. However, the X-ray structure of the NO-bound form of CcO indicates that the access of the OH groups to the bound ligand is effectively blocked by the imidazole ring of His240 as shown in Fig. 4. The X-ray structure of the CO-bound form also provides structural characteristics which are essentially the same as those of the NO-bound form [13]. These X-ray structures of CcO clearly indicate the stability of the A intermediate (the O_2-bound form).

It is well known that CO bound to Fe_{a3}^{2+} can be photolyzed and trapped at Cu_B [15]. The rebinding rate is very slow at low temperatures. Thus, at 100 K, at which X-ray diffraction experiments for the bovine heart CcO have been conducted recently, the CO-bound derivative cannot be stabilized. The X-ray structure determined at 100 K shows CO bound to Cu_B essentially in a side-on fashion [13]. The binding of CO to Cu_B at low temperatures has been examined in infrared analyses [15]. However, the binding geometry is visible in a 100 K X-ray structure at 1.8 Å resolution. The structure suggests that O_2 is trapped at Cu_B before it binds to Fe_{a3}^{2+}.

The cyanide (CN^-) bound form undergoes a fairly large conformational change in the O_2 reduction site as shown in Fig. 4B [13]. (It has been well established that the fully reduced CcO has unusually high affinity to CN^- (not HCN) [16].) At first, a fixed water bridging the Tyr244 OH group and the bound ligand is detectable concomitantly with a translational shift of the plane of heme a_3. One of the three histidine imidazole groups is released from Cu_B and CN^- forms a bridge between Fe_{a3}^{2+} and Cu_B^{1+} to form a new trigonal planar structure which includes the two imidazole groups of His240 and His291 and the bound CN^-. The plane of the new structure is perpendicular to the plane that existed before the binding of CN^-. The fixed water molecule is expected to be transferred from a water storage site located 7 Å from the O_2 reduction site. Thus, the incorporation of the water molecule concomitantly with the translational shift of the heme a_3 plane is expected to limit the rate of the conformational changes induced by cyanide.

The O_2-bound form of heme has a resonance structure between Fe^{2+}-O_2 and Fe^{3+}-O_2^-. An infrared analysis of the bound oxygen molecule suggests that the electronic structure is essentially the same as that of Fe^{3+}-O_2^- [17]. Thus, O_2 bound to Fe_{a3}^{2+}also forms Fe_{a3}^{3+}-O_2^- to induce the structural change which is essentially identical to the structural change induced by binding of CN^-. The conformational change induced by binding of O_2 provides three possible electron transfer pathways from Fe_{a3}^{3+}, Cu_B^{1+} and Tyr244-OH via the fixed water molecule. The water molecule is expected to be transferred by thermal motions of the protein moiety from the water storage site detectable about 7 Å from the O_2 reduction site in the X-ray structure [13], as in the case of the cyanide-bound fully reduced CcO, as described above. Therefore, the conformational change should be

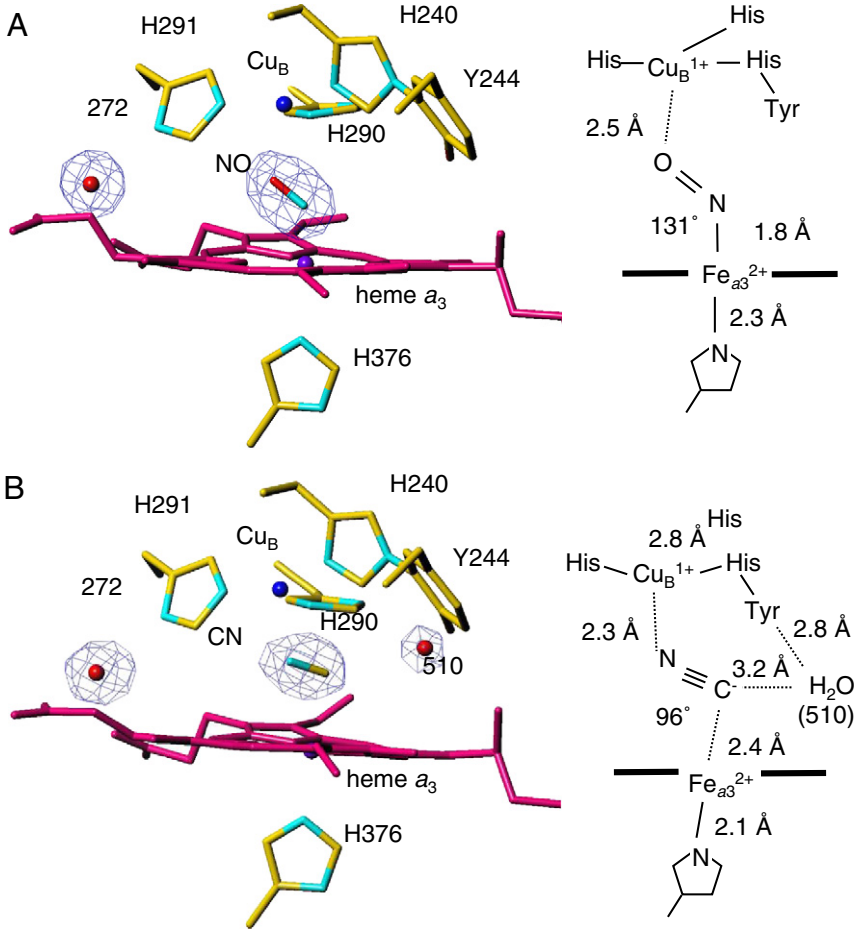

Fig. 4. The X-ray structures of the O_2 reduction sites of (A) the NO- and (B) CN^--bound forms of fully reduced CcO at 1.8 and 2.05 Å resolution, respectively. The F_O-F_C maps are contoured at (A) 6.4 σ and (B) 5.8 σ levels.The ligand-binding structures are shown in *Fo-Fc* maps. The digits without letters in the *Fo-Fc* maps indicate numbering of fixed water molecules. The structural characteristics are indicated in the schematic representations.

rate-limited by the introduction of H_2O to reduce O_2^- non-sequentially to the oxide level, without releasing any reactive oxygen species.

These results provide strong support for the O_2 reduction mechanism shown in Fig. 5 [13]. When both metals in the O_2 reduction site are in the reduced state, O_2 is introduced to Cu_B through the O_2 transfer pathway in subunit III which is controlled by the phospholipids. Cu_B traps O_2 transiently before it moves to Fe_{a3}^{2+}. The O_2 bound to Fe_{a3}^{2+} receives one electron equivalent to form O_2^-. However, before introduction of the fixed water molecule, the conformation of the O_2 reduction site is similar to that of NO-bound form. The slow introduction of the fixed water molecule increases the lifetime of the O_2 (or O_2^-) bound form so that it can be detected by resonance Raman analysis [12]. Introduction of the fixed water molecule triggers the non-sequential 3-electron reduction of O_2^- by forming the transient structure shaded in Fig. 5. This mechanism, proposed on the basis of X-ray structural analyses, could be examined by infrared spectroscopy to characterize the Cu_B-bound imidazoles and the Tyr244 OH group.

As described above, His290 is transiently removed from the Cu_B-coordination. However, it is unlikely for the imidazole group to act as a proton-pumping site, since the conformation change in His290

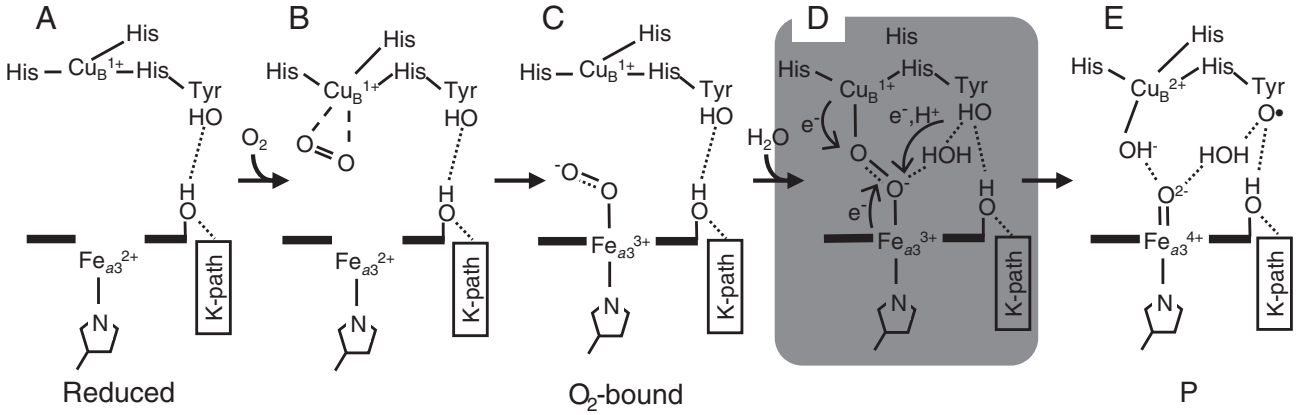

Fig. 5. A schematic representation of the O_2 reduction in CcO.The proposed intermediate is shown in the shadowed area.

is expected to occur only transiently upon O_2-binding to the fully reduced enzyme as shown in Fig. 5. No conformational change in His290 is detectable during the catalytic cycle from P to R when protons are pumped.

3.2. The structure of the resting oxidized form

As described above, under turnover conditions of CcO, the P form sequentially receives four equivalents of electrons from cytochrome *c* to produce intermediates F, O, E and R (the two electron reduced form) [2]. It has been well established that each electron transfer is coupled to the proton-pumping process to give an H^+/e^- ratio of unity [18]. The fully oxidized form, in which both metals are in the oxidized state [Fe^{3+}_{a3}-OH^-, Cu^{2+}_B-OH^-], reacts strongly and rapidly with cyanide [19]. The resonance Raman band of the O form at 450 cm^{-1} indicates Fe^{3+}_{a3}-OH^- [12]. However, under non-turnover aerobic conditions in the absence of the reducing system, another type of the oxidized form (the resting oxidized form) appears. This form is characterized by slow CN^- binding and by lacking the proton pumping function for each of the two initial electron transfers to the resting oxidized form. Comparison of the concrete structure of the O_2 reduction site of the resting oxidized form with the structure of the O form would provide a number of important insights with regard to the proton-pumping mechanism. The following experimental findings strongly support the proposal that a peroxide bridge exists between Fe^{3+}_{a3} and Cu^{2+}_B.

1) Redox titration results: it has been shown by careful redox titration analysis that 6 electron equivalents are required for complete reduction of the resting oxidized form [20]. Furthermore, a bovine heart CcO preparation which requires 4 electron equivalents for complete reduction is obtainable by oxidative titration of the fully reduced form with O_2. The O_2-oxidized CcO preparation, once exposed to air for 30 min, requires 6 electrons for complete reduction [20]. The O_2-oxidized form is likely to be identical to the fully oxidized form under turnover conditions [Fe^{3+}_{a3}-OH^-, Cu^{2+}_B-OH^-]. Thus, the reactivity of O_2 to either these metal sites would be very weak. On the other hand, it is possible that peroxide is produced from O_2 by a 2-electron donation process, induced by an irreversible modification of an amino acid residue in the protein interior. The spontaneously (and perhaps, slowly) produced peroxide would readily reacts with the fully oxidized form to provide the peroxide-bridging form [20].
2) X-ray structural results: X-ray structural analysis of the resting oxidized form was conducted by limited X-ray exposure using about 400 single crystals [21]. The hydrated electrons generated by the strong X-ray beams of SPring-8 significantly reduce the electron density of the bridging molecule between Fe_{a3} and Cu_B. The time course of the electron density decrease under the strong X-ray beams of SPring-8 was determined to extrapolate the X-ray structure to the one free from the radiation damage [21]. The extrapolated structure was determined at 1.95 Å resolution to show that a peroxide bridges the two metals in the O_2 reduction site. However, the O – O bond distance (1.7 Å) is significantly longer than the typical distance of a peroxide bridge between two metals (1.44 Å) [21].
3) Resonance Raman results: a resonance Raman band assignable to the O–O stretch of peroxide for the resting oxidized form was identified using 647.1 nm line excitation [22]. All examples of laser excitation at the shorter wavelengths appear to reduce the peroxide. Thus, many attempts to identify the O–O stretch using excitation at shorter wavelengths were unsuccessful. The isotopic shift experiments using unevenly labeled O_2 would provide important insights into the function of the O_2 reduction site.
4) Examination of the possibility of chloride-binding by anomalous dispersion analysis: it has long been proposed that a chloride ion is located between the two metals in the O_2 reduction site [23]. Considering the size of the atoms, a single chloride ion with electron density evenly distributed between the two sites would be indistinguishable from the electron density of peroxide. Thus, an anomalous dispersion analysis was applied to examine the possibility of the presence of chloride [24]. For direct elemental analysis of the O_2-reduction site, the difference anomalous electron density between Fe_{a3} and Cu_B was examined for the resting-oxidized form of bovine heart CcO using 1.7470 Å wavelength X-ray beams, which provide a slightly larger anomalous scattering factor for Cl relative to Fe and S. An anomalous peak for Cl was not detected between Cu_B and Fe_{a3} while anomalous peaks for Cu_B and Fe_{a3} were clearly detected in the same map. The result is consistent with Cl analysis (0.15 mol/mol CcO) using an ion-chromatography system after heat treatment of the crystalline CcO sample [24].

None of these experimental results, given above, is conclusive for the proposal that a peroxide bridge exists between Fe^{3+}_{a3} and Cu^{2+}_B. That is, the reductive titration does not identify the location and structure of the electron accepting site. The O – O bond distance in the X-ray structure is too long as the typical peroxide. The resonance Raman assignment has not been confirmed by the isotopic shift effect. The chloride binding has been disproved, but the analysis does not identify the structure of the bound ligand. However, presently, there would be no better structural candidate for the bridging ligand than the peroxide.

X-ray structure of the resting oxidized form indicates that two additional electron donors (Fe^{3+}_{a3} and Cu^{2+}_B) to the bound peroxide are available. The structure is definitely inconsistent to the unusual stability the resting oxidized form. Many interpretations for the stability are possible, such as a resonance stabilization of the structure [Fe^{3+}_{a3}-O^{2-}_2-Cu^{2+}_B <—> Fe^{2+}_{a3}-O_2-Cu^{1+}_B]. Elucidation of the structural basis for the stability would provide various insights in the function of the O_2 reduction site.

The initial two electron equivalents donated to the resting oxidized form are expected to reduce the bridging peroxide completely to the oxide level without affecting the oxidation states of both metals. A lag phase detected in the reductive titration curve for the resting oxidized form supports the proposal that the initial two electron equivalents reduce the bridging peroxide without reducing both metals in the O_2 reduction site [20]. Thus, the peroxide decouples the proton pump by trapping the electron equivalents to avoid reduction of the two metals. Thus, reduction of heme a_3 or Cu_B triggers the proton pump. The O_2 reduction site is not only a simple electron sink but also contributes to the proton pumping process.

3.3. Structural analyses of the proton pumping system

A redox-driven proton pumping system must have a proton-loading site demonstrating redox-coupled changes in its pK_a and accessibility (to the positive side vs the negative side), facilitated by redox-coupled conformational changes. It is impossible to evaluate the magnitude of the conformational changes required for effective proton pumping. Thus, improvement of the resolution of the X-ray structure in both oxidation states is needed for elucidation of the proton-pumping mechanism. The first redox-coupled conformational change was reported at 2.3 Å resolution in Asp51 which is located at end of the H-pathway on the positive side [14]. As shown in Fig. 6, the H-pathway includes a hydrogen-bond network and a water channel which operate in tandem. The hydrogen-bond network tightly interacts with heme *a* by forming two hydrogen-bonds with the formyl group and propionate groups of heme *a*. The water channel extends to the molecular surface of the negative side. Thus, the water molecules at the negative side surface are accessible to Arg38 at the end of the hydrogen-bond network on the negative side.

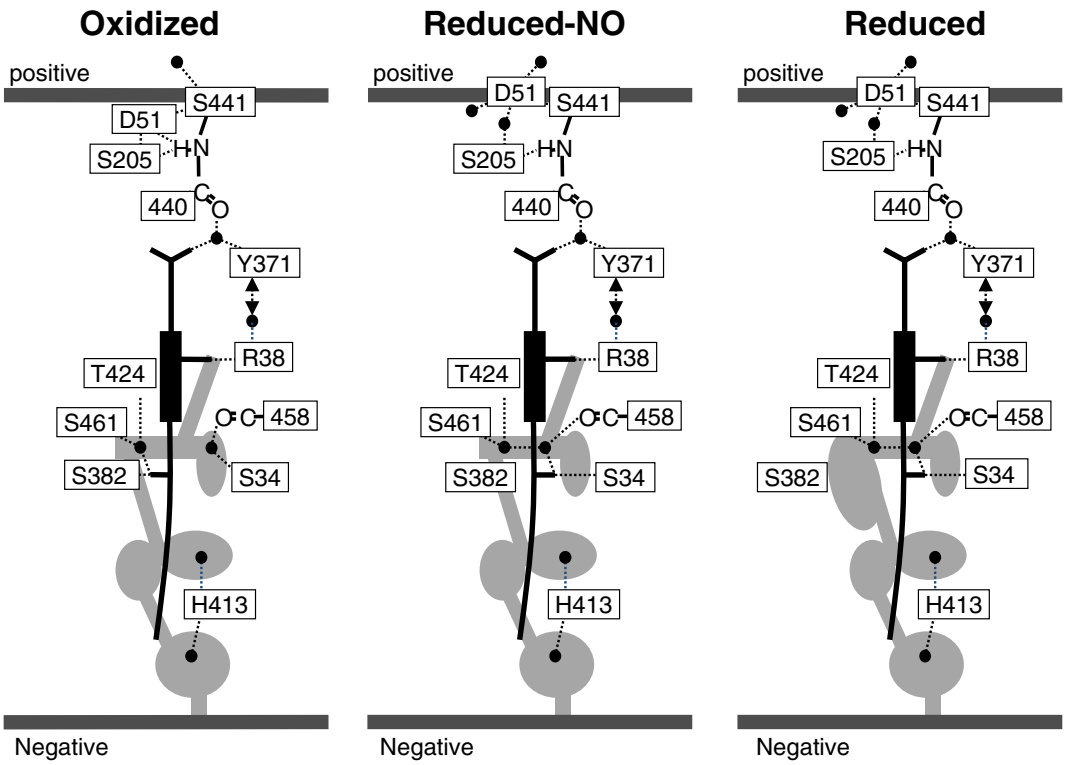

Fig. 6. Schematic representation of the structure of the H-pathway and the conformational changes induced by the oxidation state and ligand-binding state.The water channel is represented by the gray area. The black balls denote the positions of the fixed water molecules. The side view of heme a plane is shown by a rectangle with sticks which denote the peripheral groups. The dotted lines represent hydrogen bonds.

At 1.8 Å resolution, individual hydrogen atoms cannot be identified in the X-ray structure. However, the hydrogen-bonding environment clearly indicates the protonation state of acidic and basic amino acid residues [3]. The pK_a of acidic and basic amino acid residues depends upon the polarity of the solvent [25]. For example, the pK_a of acetate increases to 9 when the solvent is changed from water to methanol. As schematically shown in Fig. 7, the carboxyl group of Asp51 in the oxidized state has four hydrogen-bonds with two peptide NH groups and two Ser-OH groups, suggesting that the effective dielectric constant of the environment of the carboxyl group is quite low. Thus, the carboxyl group is mostly in the protonated state. On the other hand, in the reduced state, 3 hydrogen-bonds out of 4 are formed with water molecules [3]. Thus, the carboxyl group is predominately in the deprotonated state. The protonation state change has been confirmed by redox-difference infrared spectra which have 1585 cm^{-1} and 1738 cm^{-1} bands assignable to COO^- and COOH, respectively [3]. These bands are not detectable in bacterial CcOs which do not have an aspartate residue corresponding to Asp51. Furthermore, a reductive titration experiment for the 1585 cm^{-1} band indicates that one electron equivalent is required for the protonation state change [3]. This result is consistent with the energy transduction efficiency (H^+/e^-) of unity.

In the oxidized state, Asp51 is hydrogen-bonded to the peptide NH of Ser441. The peptide bond between Ser441 and Tyr440 is located in the H-pathway as shown in Fig. 6. Proton-transfer through a peptide bond has been well established to occur via the following mechanism [26]. A peptide C═O group can be protonated to form an imidic acid intermediate (–C(OH)═N^+H–). Then, the imidic acid releases the proton at the nitrogen atom to form the enol form of the peptide (–C(OH)═N–). Since the enol form is significantly less stable than the keto form, the enol form is spontaneously transformed to the keto form (–CO–NH–). Thus, the proton transfer must be unidirectional. The peptide bond is expected to block the backward leakage of protons from the positive side.

It should be noted that the enol/keto transition is likely to be restricted for the tightly fixed peptide bond within the interior of the protein. Thus, the transition could be driven by deprotonation of the OH group and protonation of the nitrogen atom on both sides of the peptide. Then, no net proton transfer would occur through the peptide bond. The possibility of net proton transfer through the peptide bond between Ser441 and Tyr440 in the bovine heart CcO was examined theoretically taking into account the X-ray structure near the peptide bond. The careful calculation shows that proton transfer through the peptide bond between Ser441 and Tyr440 is possible within the physiological time scale [27].

In the reduced state, heme *a* has no net charge since the positive charge of Fe_a^{2+} is neutralized by the two negative charges of the porphyrin moiety. Upon oxidation, Fe_a creates one equivalent of net positive charge. The fact that there is no redox-coupled structural change in heme *a* in the X-ray structure at 1.8 Å resolution suggests that the net positive charge is not neutralized by uptake of an anion. If heme *a* were in aqueous solution, an anion such as Cl^- or OH^- would be taken up to compensate for (or neutralize) the positive charge increase. Thus, a significant amount of positive charge delocalization is expected to occur over the formyl and propionate groups. The delocalized net positive charge drives active proton transport through the hydrogen-bond network. The large positive charge increase in the formyl group which occurs upon oxidation was demonstrated in 1989 by observing a resonance Raman C–O stretch shift from 1610 cm^{-1} to 1650 cm^{-1}, which is assignable to the formyl group of heme *a* and not heme a_3 [28]. A change in the strength of hydrogen bonding to the formyl group also is expected to induce the band shift. Thus, these X-ray structures of the hydrogen-bond network strongly suggest that this is the coupling site between O_2 reduction and proton pumping.

The water channel of the H-pathway, identified by a molecular surface calculation, includes a water pathway and a water cavity [3]. The water pathway is too narrow to permit a stable accumulation of

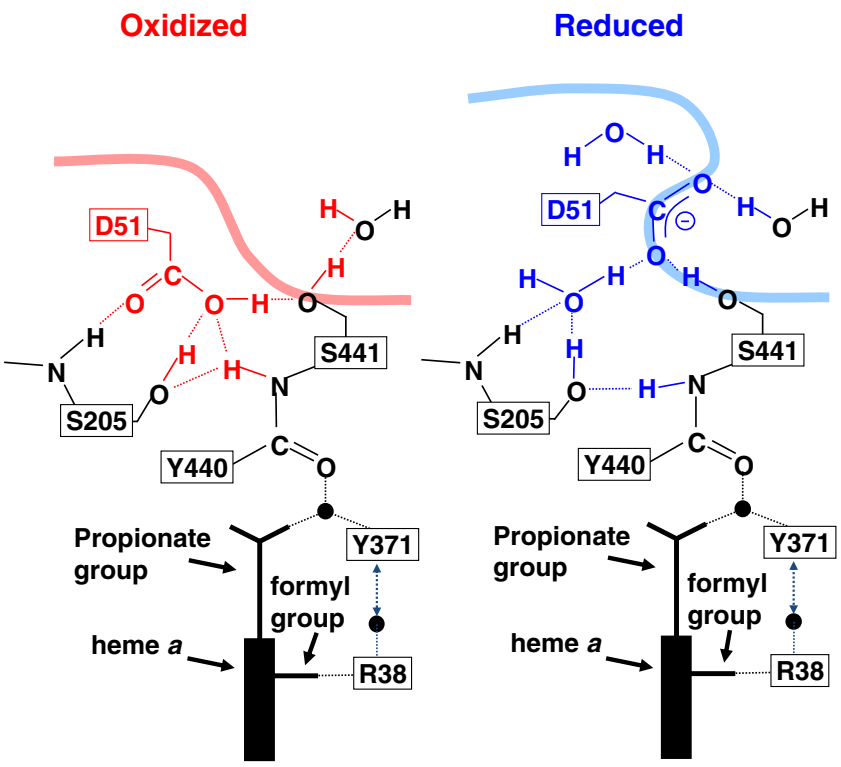

Fig. 7. Schematic representation of the hydrogen-bonding structure of Asp51 in the oxidized (Left) and reduced (Right) states.The smooth thick curve denotes the molecular surface to which the water molecules in the positive side space are accessible. The conformational changes upon reduction are shown by blue structures in the light panel. The black balls and dotted lines represent the fixed water molecules and hydrogen bonds, respectively.

water molecules. At least one water molecule can be stored in the water cavity, as schematically represented in Fig. 6. The water cavities distributed in the water channel promote the water-exchange inside the water channel and thus proton-equilibration between the negative side phase and Arg38, which is located at the end of the hydrogen bond network on the negative side. However, the largest cavity detectable in the reduced state is eliminated upon oxidation of the O_2 reduction site, as shown in Fig. 6, by a conformational change in a transmembrane α-helix located between the planes of the two hemes [3]. The significant narrowing of the water channel, which elongates the water pathway, is strongly expected to decrease the efficiency of the water-exchange inside the water channel. Thus, water exchange as well as backward leakage of protons from the hydrogen-bond network would be blocked within the physiological time scale. The conformations in the oxidized and reduced states are designated as the closed and open states, respectively.

X-ray structural analyses of various O_2 analog derivatives show that the channel is also closed upon binding of strong ligands to Fe_{a3}^{2+}, such as CO and NO, while weak ligands such as CN^- do not induce the conformational change [13]. Thus, O_2 binding is expected to result in closure of the water channel. Preliminary X-ray structural analysis shows that the water channel is also in the closed conformation in the intermediate species P, F, and O. Although no X-ray structural information for E is presently available, a kinetic analysis of single electron reduction of the O state strongly suggests that the electron equivalent is located at Cu_B in the E intermediate [29]. An oxidation state of Fe_{a3} higher than 3+ is likely to provide the closed conformation since, P ($Fa_{a3}^{5+}=O^{2-}$), F ($Fa_{a3}^{4+}=O^{2-}$), O (Fa_{a3}^{3+}-OH^-), and the resting oxidized (O_R) form (Fa_{a3}^{3+}-O-O) each adopt the closed conformation. Intermediate E is expected to be in the closed state. Therefore, the water channel is in the open state only when the O_2 reduction site is in the ligand-free reduced state. As described above, proton pumping is coupled to each of the four one-electron transfer processes from cytochrome *c* to the O_2 reduction site after formation of the P intermediate, to regenerate R form. During the catalytic cycle, the closed conformation during the transition from A to R is expected to effectively block any backward leakage of protons from the hydrogen bond network. Thus, the backward leakage of protons is blocked at two points, the peptide bond and the water channel. To obtain efficient energy transduction of $H^+/e^-=1$, four proton equivalents must be collected in the hydrogen-bond network when the water channel is open (during the transition of intermediate R to intermediate A), as schematically shown by Fig. 8. The structure of the hydrogen-bond network suggests that the collection of 4 proton equivalents is not a rapid process. Thus, there must be a system for appropriate control of O_2 binding for complete collection of protons to be used in the pumping process.

3.4. Structural analyses of one of the proton conducting pathways extending from the O_2 reduction site to the molecular surface on the negative side

Bovine heart CcO has two additional proton conducting pathways known as the D- and K-pathways. These pathways extend from the surface of the negative side to the O_2 reduction site and are expected to be involved in transfer of protons used to generate water molecules. The structures of these pathways are well conserved in eukaryotic and prokaryotic cells. Replacement of the critical acidic amino acid residues in D-pathway of bacterial enzymes with their amide forms (for example, Glu to Gln) results in blockage of both electron transfer and proton pumping activities, indicating that proton transfer through the D-pathway is tightly coupled to the electron transfer to the O_2 reduction site which drives the proton pumping process [30]. Furthermore, these processes (electron transfer, proton pumping and proton transfer for water formation) are expected to be tightly coupled to each other to enable effective energy transduction. In order to identify the structural basis for these coupling mechanisms, improvement of the resolution of X-ray structure is needed.

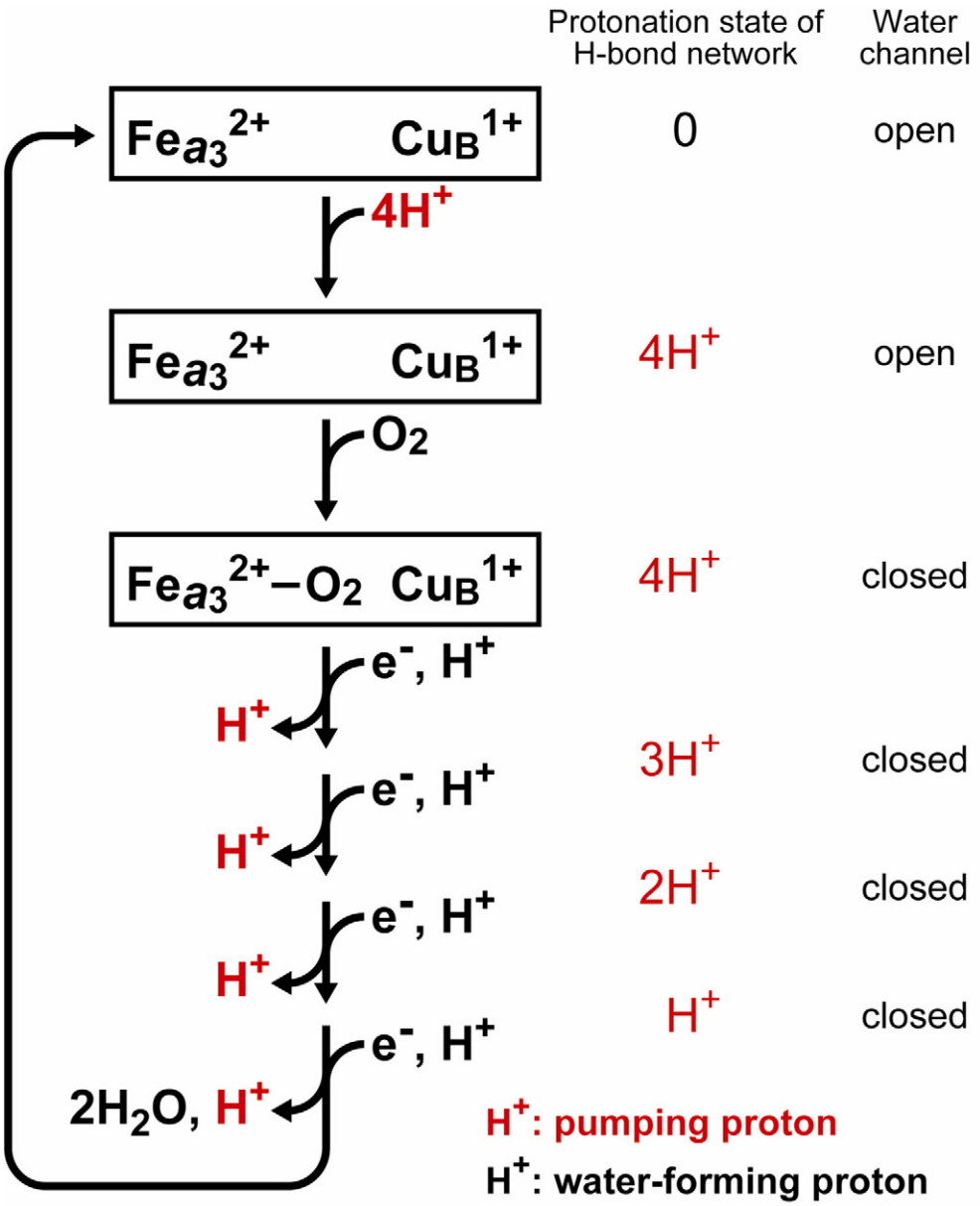

Fig. 8. Schematic representation of the catalytic cycle of bovine heart cytochrome *c* oxidase.

High resolution X-ray structural analysis shows a redox-coupled 180° rotation of the imidazole ring of His503 at the entrance of the D-pathway, suggesting the existence of a proton collection process wherein protons from the negative side space are transferred to the D-pathway [31], as schematically shown in Fig. 9. It is possible that a water molecule is trapped by hydrogen bonds between His503 and Asp91 of the D-pathway and becomes linked with the molecular surface via two water arrays in the reduced state. The microenvironment of Asp91 in the X-ray structure strongly suggests that the proton affinity is as high as that of His503 which is essentially exposed to the bulk water phase. These two amino acid residues trap a proton equivalent from the bulk water phase on the negative side by stabilizing the hydronium ion state of the water. Upon oxidation, the imidazole ring rotates by 180° causing breakage of the hydrogen-bond to the protonated water. Then, the proton equivalent on the fixed water molecule is released to Asp91 which transfers the proton to the O_2 reduction site through the D-pathway to neutralize the negative charge transferred by the electron. The proton collection function has been confirmed by the observation that binding of Zn^{2+} and Cd^{2+} to His503 partially inhibits the O_2 reduction function. The estimated K_d for binding of Zn^{2+} in the X-ray structure is consistent with the reported K_d for complete proton pumping inhibition by Zn^{2+}[32]. A recently reported careful analysis for the effect of zinc-binding to the negative side on the proton pumping of bovine heart CcO shows that internally trapped Zn^{2+} provides 50% decoupling of the proton pump at level flow [33]. The zinc concentration required for the decoupling suggests that Zn^{2+} binding to His503 induces the decoupling. These results suggest the existence of coupling via His503 between proton transfer for O_2 reduction and proton pumping.

4. Mutational analysis of the proton-pumping system of the bovine heart CcO

The extensive X-ray structural analyses described above suggest that the H-pathway pumps protons via a mechanism driven by oxidation of heme *a*. However, this proposal, deduced from X-ray structural analyses, should be examined by functional analyses of the H-pathway. Here recent progress in mutational analysis of the H-

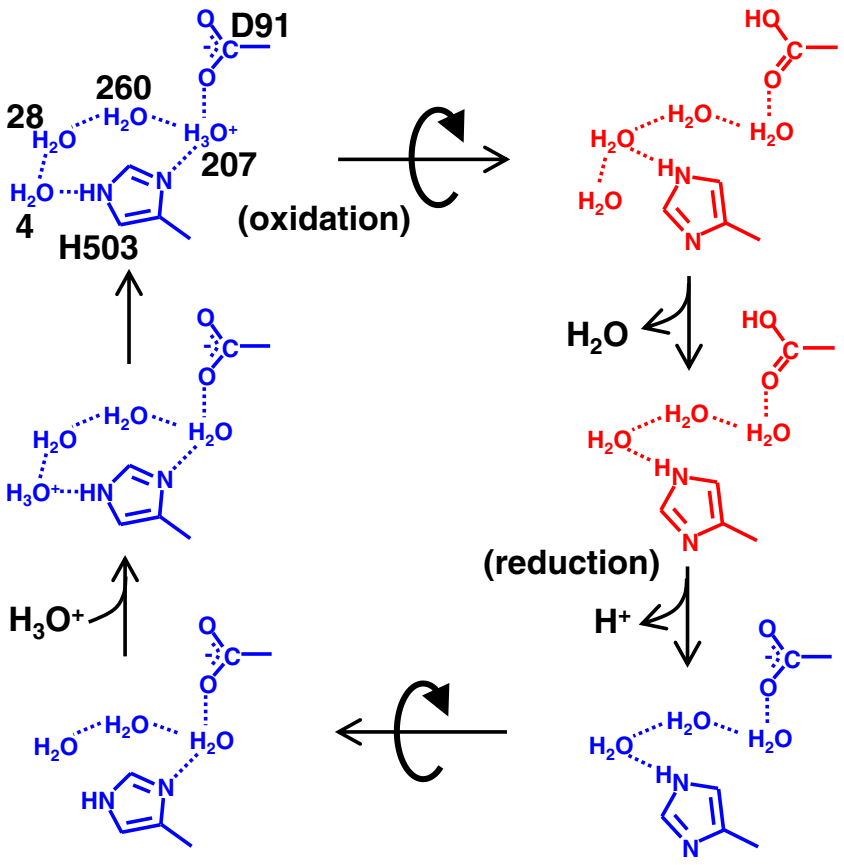

Fig. 9. Redox-coupled proton collection and supply by His503.The red and blue structures represent the oxidized and reduced states of the redox site controlling the conformation of the imidazole of His503.

pathway of bovine heart CcO is summarized and compared with a proton-pumping mechanism deduced from mutational analyses of bacterial CcOs.

Using a stable expression system we constructed for subunit I of the bovine heart CcO gene, which includes all amino acid residues of the H-pathway, site directed mutagenesis was performed at three critical points of the H-pathway [3,4]. Asp51Asn was generated to block the end of the H-pathway at the positive side, Tyr440Pro was constructed to block proton transfer through the peptide bond in the hydrogen bond network, and a double mutation, Val386Leu/Met390Trp was generated to block the water pathway by providing bulkier residues. As is well known, a proline mutation often destroys the original protein conformation and thus makes straightforward interpretation of the mutation results extremely difficult. However, the dihedral angle of the peptide bond between Tyr440 and Ser441 suggests that only a minimal conformational change is induced by the mutation [4].

The three different types of mutation provide an identical phenotype characterized by abolishment of proton pumping without decreasing the O_2 reduction activity. These results clearly confirm that the H-pathway is involved in proton-pumping. The hydrogen-bond network and heme *a* system connected by the two hydrogen-bonds described above acts as the coupling site between electron transfer and proton-pumping. This may represent the first concrete coupling proposal. The structure suggests that blockage of proton transfer through the hydrogen bond network would not block electron transfer, since electron transfer is driven by O_2 reduction accompanied by a large free energy change. Another important point of the mechanism of proton pumping through the H-pathway is that the proton pumping pathway is completely isolated from the pathway traveled by protons used to form water molecules. Without isolation of the proton-pumping system from the water forming proton pathway, protons used in the pumping process could also be used to form water molecules. This would dissipate the free energy change due to O_2 reduction, as suggested long ago [34]. If both the proton pathways are not isolated completely, a functional gate is required for effective energy transduction.

Asp51 in the H-pathway is conserved in most mammalian CcOs but plant and bacterial CcOs do not have this residue. On the other hand, the structure of the D-pathway is quite well conserved among many species including bacterial CcOs. Thus, a mechanism of pumping protons through the D-pathway has been proposed, based on site directed mutagenesis experiments. Mutations of critical polar amino acid residues of the D-pathway abolish both proton and electron transfer activities [30]. The Asn139Asp mutation (with reference to *R. sphaeroides*) in the D-pathway abolishes proton pumping without decreasing O_2 reduction activity [35]. Based on these results, it has been proposed that the D-pathway transfers protons used for pumping and for generating water molecules. However, it should be noted that abolishment of both proton pumping and O_2 reduction activities by the D-pathway mutations do not provide conclusive evidence that these pathways are used to transfer protons used for pumping and for generating water molecules. An equally possible interpretation for the abolishment of both proton and electron transfer activities is that proton transfer for water formation through D-pathway is tightly coupled to electron transfer to the O_2 reduction site. Without O_2 reduction, proton pumping is not possible. Furthermore, replacement of Asn139 in the D-pathway with Asp is unlikely to block proton transfer through the D-pathway, since both Asn and Asp can participate in a proton transfer pathway by forming hydrogen bonds with adjacent groups in the D-pathway. This result simply suggests that the Asn/Asp exchange influences the proton pumping site

to abolish the proton pump. However, the mutation result does not identify the proton pumping site. Conclusive experimental (non-empirical) evidence for proton-pumping via the D-pathway is needed. On the other hand, all the structural changes induced by the three bovine heart CcO mutations, Asp51Asn, Tyr440Pro and Val386-leu/met390Trp are most likely to block the proton transfer at the mutation site. For example, Asp51 accepts and releases pumping protons in the oxidized and reduced states, respectively. That is, Asp51 must be in the protonated state (−COOH) in the oxidized state, while Asn51is not able to receive protons stably in the oxidized state. Thus, the simples interpretation for the mutation results is that Asn51 itself blocks the proton transfer driven by Asp51 in the wild type CcO.

It has been recently reported that even the D-pathway is not completely conserved among all heme-copper oxygen reductases [36,37]. The common elements across all families of the heme-copper oxygen reductases include the heme a_3/Cu_B dinuclear site, the four histidine imidazole groups that coordinate the metals and the covalently linked His-Tyr moiety. Thus, it has been suggested that the only roles of these channels are in proton delivery. However, an alternative interpretation is possible to explain this diversity. Reduction of O_2 without release of any reactive oxygen species must be a well-organized complex reaction process. No alternative system with higher efficiency than the Fe_{a3}/Cu_B system has been developed during the course of evolution of aerobic organisms. On the other hand, since proton pumping is a chemically simple reaction, various amino acid residues can facilitate the pumping function to provide diversity in the proton pumping mechanism. In fact, the diversity in proton-pumping efficiency is most likely to be induced by the diversity in the proton-pumping mechanism.

Acknowledgements

This work is supported in part by the Grant-in-Aid for Scientific Research 2247012 (S.Y.), the Targeted Protein Research Program, and the Global Center of Excellence Program, each provided by the Japanese Ministry of Education, Culture, Sports, Science and Technology. S.Y. is a Senior Visiting Scientist in the RIKEN Harima Institute.

References

[1] E. Yakushiji, K. Okunuki, Isolierung der a-Komponente des Cytochroms und ihre Eigenschaften, Proc. Imp. Acad. Jpn. 17 (1941) 38–40.
[2] S. Yoshikawa, K. Muramoto, K. Shinzawa-Itoh, Proton-pumping mechanism of cytochrome *c* oxidase, Annu. Rev. Biophys. 40 (2011) 205–223.
[3] T. Tsukihara, K. Shimokata, Y. Katayama, H. Shimada, K. Muramoto, H. Aoyama, M. Mochizuki, K. Shinzawa-Itoh, E. Yamashita, M. Yao, Y. Ishimura, S. Yoshikawa, The low-spin heme of cytochrome *c* oxidase as the driving element of the proton-pumping process, Proc. Natl. Acad. Sci. U. S. A. 100 (2003) 15304–15309.
[4] K. Shimokata, Y. Katayama, H. Murayama, M. Suematsu, T. Tsukihara, K. Muramoto, H. Aoyama, S. Yoshikawa, H. Shimada, The proton pumping pathway of bovine heart cytochrome *c* oxidase, Proc. Natl. Acad. Sci. U. S. A. 104 (2007) 4200–4205.
[5] B. Kadenbach, M. Ungibauer, J. Jarausch, U. Buge, L. Kuhn-Nentwig, The complexity of respiratory complexes, Trends Biochem. Sci. 8 (1983) 398–400.
[6] T. Tsukihara, H. Aoyama, E. Yamashita, T. Tomizaki, H. Yamaguchi, K. Shinzawa-Itoh, R. Nakashima, R. Yaono, S. Yoshikawa, The whole structure of the 13-subunit oxidized cytochrome *c* oxidase at 2.8 A, Science 272 (1996) 1136–1144.
[7] K. Shinzawa-Itoh, H. Aoyama, K. Muramoto, H. Terada, T. Kurauchi, Y. Tadehara, A. Yamasaki, T. Sugimura, S. Kurono, K. Tsujimoto, T. Mizushima, E. Yamashita, T. Tsukihara, S. Yoshikawa, Structures and physiological roles of all the integral lipids of bovine heart cytochrome *c* oxidase, EMBO J. 26 (2007) 1713–1725.
[8] N.C. Robinson, Specificity and binding affinity of phospholipids to the high-affinity cardiolipin sites of beef heart cytochrome *c* oxidase, Biochemistry 21 (1982) 184–188.
[9] G. Gilderson, L. Salomonson, A. Aagaard, J. Gray, P. Brzezinski, J. Hosler, Subunit III of cytochrome *c* oxidase of *Rhodobacter sphaeroides* is required to maintain rapid proton uptake through the D pathway at physiological pH, Biochemistry 42 (2003) 7400–7409.
[10] W.S. Caughey, G.A. Smythe, D.H. O'Keefe, J.E. Maskasky, M.L. Smith, Heme A of cytochrome *c* oxidase, J. Biol. Chem. 250 (1975) 7602–7622.
[11] E. Yamashita, H. Aoyama, M. Yao, K. Muramoto, K. Shinzawa-Itoh, S. Yoshikawa, T. Tsukihara, Absolute configuration of the hydroxy-farnesylethyl group of heme A, determined by X-ray structural analysis of bovine heart cytochrome *c* oxidase using a novel method applicable at 2.8 Å resolution, Acta Crystallogr. D61 (2005) 1373–1377.
[12] T. Kitagawa, T. Ogura, Oxygen activation mechanism at the binuclear site of heme-copper oxidase superfamily as revealed by time-resolved resonance Raman spectroscopy, Prog. Inorg. Chem. 45 (1997) 431–479.
[13] K. Muramoto, K. Ohta, K. Shinzawa-Itoh, K. Kanda, M. Taniguchi, H. Nabekura, E. Yamashita, T. Tsukihara, S. Yoshikawa, Bovine cytochrome *c* oxidase structures enable O_2 reduction with minimization of reactive oxygens and provide a proton-pumping gate, Proc. Natl. Acad. Sci. U. S. A. 107 (2010) 7740–7745.
[14] S. Yoshikawa, K. Shinzawa-Itoh, R. Nakashima, R. Yaono, E. Yamashita, N. Inoue, M. Yao, M.J. Fei, C. Peters Libeu, T. Mizushima, H. Yamaguchi, T. Tomizaki, H. Yamaguchi, T. Tsukihara, Redox-coupled crystal structural changes in bovine heart cytochrome *c* oxidase, Science 280 (1998) 1723–1729.
[15] F.G. Fiamingo, R.A. Altshuld, P.P. Moh, J.O. Alben, Dynamic interaction of CO with a_3Fe and Cu_B in cytochrome *c* oxidase in beef heart mitochondria studied by Fourier transform infrared spectroscopy at low temperatures, J. Biol. Chem. 257 (1982) 1639–1650.
[16] S. Yoshikawa, M. Mochizuki, X.-J. Zhao, W.S. Caughey, Effects of overall oxidation state on infrared spectra of heme a_3 cyanide in bovine heart cytochrome *c* oxidase, J. Biol. Chem. 270 (1995) 4270–4279.
[17] W.T. Potter, M.P. Tucker, R.A. Houtchens, W.S. Caughey, Oxygen infrared spectra of oxyhemoglobins and oxymyoglobins. Evidence of two major O_2 structures, Biochemistry 26 (1987) 4699–4707.
[18] D. Bloch, I. Belevich, A. Jasaitis, C. Ribacka, A. Puustinen, M.I. Verkhovsky, M. Wikstrom, The catalytic cycle of cytochrome *c* oxidase is not the sum of its two halves, Proc. Natl. Acad. Sci. U. S. A. 101 (2004) 529–533.
[19] P.E. Thornstrom, T. Nilsson, B.G. Malmstrom, The possible role of the closed-open transition in proton pumping by cytochrome *c* oxidase:The pH dependence of cyanide inhibition, Biochim. Biophys. Acta 935 (1988) 103–108.
[20] M. Mochizuki, H. Aoyama, K. Shinzawa-Itoh, T. Usui, T. Tsukihara, S. Yoshikawa, Quantitative reevaluation of the redox active sites of crystalline bovine heart cytochrome *c* oxidase, J. Biol. Chem. 274 (1999) 33403–33411.
[21] H. Aoyama, K. Muramoto, K. Shinzawa-Itoh, K. Hirata, E. Yamashita, T. Tsukihara, T. Ogura, S. Yoshikawa, A Peroxide bridge between Fe and Cu ions in the O_2 reduction site of fully oxidized cytochrome *c* oxidase could suppress the oroton oump, Proc. Natl. Acad. Sci. U. S. A. 106 (2009) 2165–2169.
[22] M. Sakaguchi, K. Shinzawa-Itoh, S. Yoshikawa, T. Ogura, A resonance Raman band assignable to the O–O stretching mode in the resting oxidized state of bovine heart cytochrome *c* oxidase, J. Bioenerg. Biomembr. 42 (2010) 241–243.
[23] M. Fabian, L. Skultety, C. Brunel, G. Palmer, Cyanide stimulated dissociation of chloride from the catalytic center of oxidized cytochrome *c* oxidase, Biochemistry 40 (2001) 6061–6069.
[24] M. Suga, N. Yano, K. Muramoto, K. Shinzawa-Itoh, T. Maeda, E. Yamashita, T. Tsukihara, S. Yoshikawa, Distinguishing between Cl^- and O_2^{2-} as the bridging element between Fe^{3+} and Cu^{2+} in the resting oxidized cytochrome *c* oxidase, Acta Crystallogr. D67 (2011) 742–744.
[25] N.S. Isaacs, Physical Organic Chemistry, second ed. Longman, Essex, 1995.
[26] C.L. Perrin, Proton exchange in amides: surprise from single systems, Acc. Chem. Res. 22 (1989) 268–275.
[27] K. Kamiya, M. Boero, M. Tateno, K. Shiraishi, A. Oshiyama, Possible mechanism of proton transfer through peptide groups in the H-pathway of the bovine cytochrome *c* oxidase, J. Am. Chem. Soc. 129 (2007) 9663–9673.
[28] M. Sasaroli, Y.-C. Ching, S. Dasgupta, D.L. Rousseau, Cytochrome *c* oxidase: evidence for interaction of water molecules with cytochrome *a*, Biochemistry 28 (1989) 3128–3132.
[29] I. Belevich, D.A. Bloch, N. Belevich, M. Wikstrom, M.I. Verkhovsky, Exploring the proton pump mechanism of cytochrome *c* oxidase in real time, Proc. Natl. Acad. Sci. U. S. A. 104 (2007) 2685–2690.
[30] A. Konstantinov, S. Siletsky, D. Mitchell, A. Kaulen, R.B. Gennis, The roles of the two proton input channels in cytochrome *c* oxidase from *Rhodobacter sphaeroides* probed by the effects of site-directed mutations on time-resolved electrogenic intraprotein proton transfer, Proc. Natl. Acad. Sci. U. S. A. 94 (1997) 9085–9090.
[31] K. Muramoto, K. Hirata, K. Shinzawa-Itoh, S. Yoko-o, E. Yamashita, H. Aoyama, T. Tsukihara, S. Yoshikawa, A histidine residue acting as a controlling site for dioxygen reduction and proton pumping by cytochrome *c* oxidase, Proc. Natl. Acad. Sci. U. S. A. 104 (2007) 7881–7886.
[32] A. Kannt, T. Ostermann, H. Muller, M. Ruitenberg, Zn^{2+} binding to the cytoplasmic side of *Paracoccus denitrificans* cytochrome c oxidase selectively uncouples electron transfers and proton translocation, FEBS Lett. 503 (2001) 142–146.
[33] P.L. Martino, G. Capitanio, N. Capitanio, S. Papa, Inhibition of proton pumping in membrane reconstituted bovine heart cytochrome *c* oxidase by zinc binding at the inner matrix side, Biochim. Biophys. Acta 1807 (2011) 1075–1082.
[34] R.J.P. Williams, Puropose of proton pathways, Nature 376 (1995) 643.
[35] A.S. Pawate, J. Morgan, A. Namslauer, D. Mills, P. Brzenzinski, S. Ferguson-Miller, R.B. Gennis, A mutation in subunit I of cytochrome oxidase from *Rhodobacter sphaeroides* results in an increase in steady-state activity but completely eliminates proton pumping, Biochemistry 41 (2002) 13417–13423.
[36] H.Y. Chang, J. Hemp, Y. Chen, J.A. Fee, R.B. Gennis, The cytochrome ba_3 oxygen reductase from *Thermus thermophilus* uses a single input channel for proton delivery to the active site and for proton pumping, Proc. Natl. Acad. Sci. U. S. A. 106 (2009) 16169–16173.
[37] J. Hemp, H. Han, J.H. Roh, S. Kaplan, T.J. Martinez, R.B. Gennis, Comparative genomics and site-directed mutagenesis support the existence of only one input channel for protons in the C-family (cbb_3 Oxidase) of heme-copper oxygen reductases, Biochemistry 46 (2007) 9963–9972.